IEEE Photonics Journal
An IEEE Photonics Society Publication

Open Access

Enhancement of Hole Confinement by Monolayer Insertion in Asymmetric Quantum-Barrier UVB Light Emitting Diodes

Volume 6, Number 2, April 2014

Bilal Janjua
T. K. Ng, Member, IEEE
Ahmed Y. Alyamani
M. M. El-Desouki
B. S. Ooi, Senior Member, IEEE

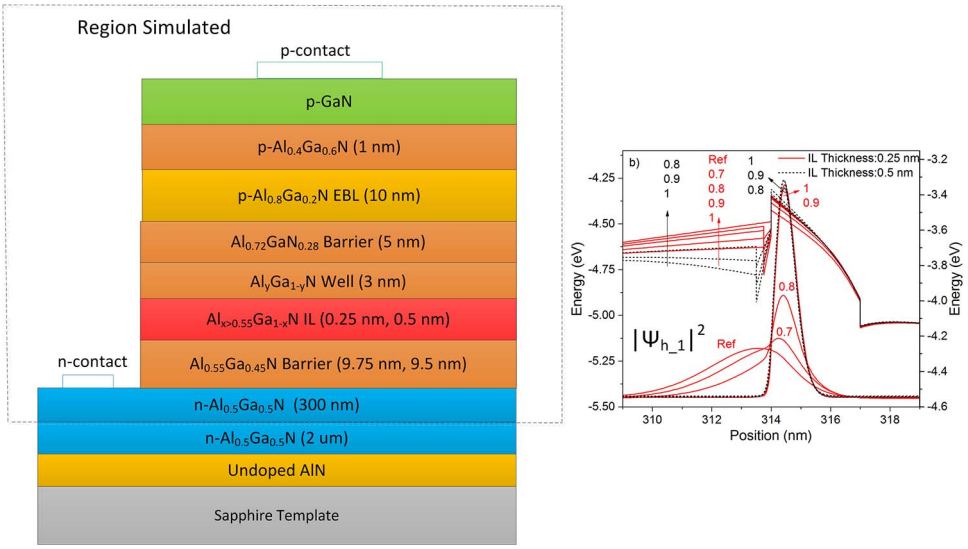

DOI: 10.1109/JPHOT.2014.2310199
1943-0655 © 2014 IEEE

Enhancement of Hole Confinement by Monolayer Insertion in Asymmetric Quantum-Barrier UVB Light Emitting Diodes

Bilal Janjua,[1] T. K. Ng,[1] *Member, IEEE*, Ahmed Y. Alyamani,[2] M. M. El-Desouki,[2] and B. S. Ooi,[1] *Senior Member, IEEE*

[1]Photonics Laboratory, Computer, Electrical and Mathematical Sciences and Engineering (CEMSE) Division, King Abdullah University of Science & Technology (KAUST), Thuwal 23955-6900, Saudi Arabia
[2]National Center for Nanotechnology, King Abdulaziz City for Science and Technology (KACST), Riyadh 11442-6086, Saudi Arabia

DOI: 10.1109/JPHOT.2014.2310199

Manuscript received January 21, 2014; revised February 25, 2014; accepted March 1, 2014. Date of publication March 6, 2014; date of current version March 19, 2014. This work was supported by King Abdulaziz City for Science and Technology (KACST) under the Technology Innovation Center (TIC) program. Corresponding author: B. S. Ooi (e-mail: boon.ooi@kaust.edu.sa).

Abstract: We study the enhanced hole confinement by having a large bandgap AlGaN monolayer insertion (MLI) between the quantum well (QW) and the quantum barrier (QB). The numerical analysis examines the energy band alignment diagrams, using a self-consistent 6×6 $k \cdot p$ method and, considering carrier distribution, recombination rates (*Shockley–Reed–Hall, Auger*, and radiative recombination rates), under equilibrium and forward bias conditions. The active region is based on $Al_aGa_{1-a}N$ (barrier)/$Al_bGa_{1-b}N$ (MLI)/$Al_cGa_{1-c}N$ (well)/$Al_dGa_{1-d}N$ (barrier), where $b > d > a > c$. A large bandgap $Al_bGa_{1-b}N$ mono layer, inserted between the QW and QB, was found to be effective in providing stronger hole confinement. With the proposed band engineering scheme, an increase of more than 30% in spatial overlap of carrier wavefunction was obtained, with a considerable increase in carrier density and direct radiative recombination rates. The single-QW-based UV-LED was designed to emit at 280 nm, which is an effective wavelength for water disinfection.

Index Terms: Light emitting diodes (LEDs), semiconductor quantum well, wavefunction overlap, thin insertion layer, energy barrier, ultraviolet, water disinfection.

1. Introduction

AlGaN based UV LEDs have attracted great attention for applications in environmental purification, medicine, lighting and vitamin B3 generation in human body [1]. However, due to the large polarization fields, the illumination power and internal quantum efficiency (IQE) of nitride based devices is low [2]–[5]. The improvement in carrier recombination rate and increase in radiative recombination efficiency, in such UV LEDs, remains a great challenge. Novel designs to enhance optical matrix element have been demonstrated [6]–[8]. To date, UV LEDs development is championed by SETi Corporation with record external efficiency greater than 11% at 278 nm emission wavelength [9]. The design rules are not well established due to complex interaction between polarization fields, lattice strain and bandgap engineering. These issues hence warrant a careful device design simulation of the layer structure before actual layer structure growth

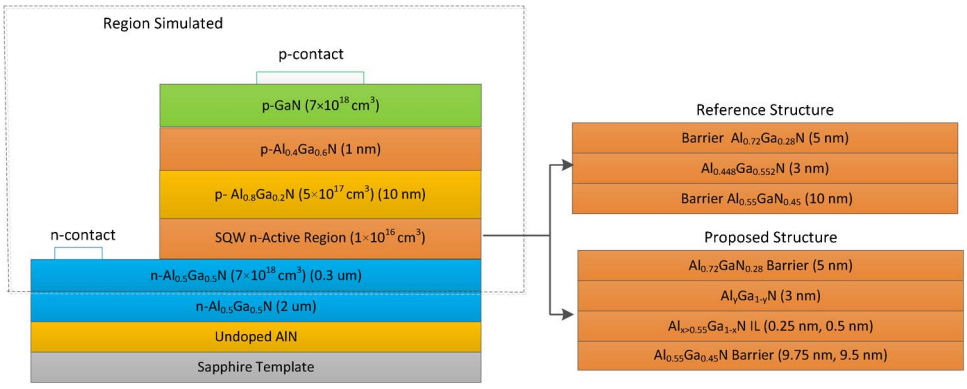

Fig. 1. Schematics of the full UVB LED structure, the reference structure design, and the proposed structure design with thin AlGaN monolayer insertion (MLI).

implementation. Design based on the practical growth related boundary conditions is also vital to the usefulness of a simulation. This paper explores the thin barrier insertion layer design with eventual view of realizing the design using plasma source molecular beam epitaxy (PSMBE), which has a controllable monolayer (ML) growth capability.

The major cause of reduced internal quantum efficiency (IQE) in nitride based devices, is the large band bending caused by high internal polarization fields, close to several MV/cm, in the active regions [10]–[12]. Band bending results in reduced oscillator strength of carrier recombination, a dimensionless quantity expressing the strength of direct transitions, and the quantum confined Stark effect (QCSE). This creates a major challenge in emitter device design on polar c-plane substrates. Small valence band offset in AlGaN based hetero-structures results in weak hole confinement for devices based on single quantum well (SQW) design. Weak confinement can lead to hole leakage into the n-cladding, resulting in undesirable recombination process. To improve IQE, proposal based on inserting carrier-confinement barrier layer AlGaInN and InGaN based active regions for visible wavelengths were reported [13], [14]. A similar technique for UV LEDs design is currently lacking, and requires further study and optimization. Moreover, such designs are yet to be fully developed in conjunction with AlGaN QW device grown using PSMBE, which can achieve a controllable growth rate of < 1 nm per minute, favoring the implementation of the insertion of few monolayers in the active region.

In this investigation, the design of AlGaN ML insertions (AlGaN-MLI), has been studied numerically. The numerical analysis considered energy band alignment, comparison of carrier densities in QW, wavefunction spatial overlap, recombination rates and tunneling probability. AlGaN-MLI, thickness and alloy composition were optimized to achieve largest wavefunction overlap. Comparing conventional active region design with the proposed structure, we found more than 30% enhancement in spatial overlap of wavefunctions using $Al_aGa_{1-a}N$ (barrier) / $Al_bGa_{1-b}N$ (MLI) / $Al_cGa_{1-c}N$ (well) / $Al_dGa_{1-d}N$ (barrier), where $b > d > a > c$, as the active region. The proposed designed was modeled using the NEXTNANO software [15]. The band diagram of the structure was obtained by solving Poisson's, Schrödinger, current continuity, carrier transport and photon rate equations, self-consistently. The wavefunction overlap, carrier dynamics in AlGaN based active region, polarization induced band bending due to interface fixed charges were considered. The proposed UV-LED is designed to emit at 280 nm, which is an attractive wavelength for water disinfection applications.

2. Numerical Simulation Setup

The proposed design based on $Al_aGa_{1-a}N/Al_{1-b}GaN/Al_{1-c}GaN/Al_{1-d}GaN$, where $b > d > a > c$, active region, is shown in Fig. 1. The LED modeled in this study consists of a 300 nm $Al_{0.5}Ga_{0.5}N$ layer, n doped, with carrier concentration of 7×10^{18} cm^3. The active region consists of $Al_{0.55}Ga_{0.45}N$

TABLE 1
Material properties of the binary used in the simulation considering bowing parameters

Material	E_g (eV) at 0K	a (nm)	c (nm)	Spontaneous Polarization (C/m^2)
AlN	6.1	0.3112	0.4982	-0.0898
GaN	3.51	0.31892	0.5185	-0.0339
Bowing factor (b)	0.8	-0.007	0.039	-0.021

bottom barrier layer, followed by the monolayer insertion. Thickness of the bottom barrier including MIL is kept at 10 nm. Next to MIL is a 3 nm $Al_{1-y}Ga_{1-y}N$ QW terminated with a 5 nm $Al_{0.72}Ga_{0.28}N$ top barrier. The asymmetric barrier design was chosen due to the difference in mobility of holes in each intrinsic layer. The active region is assigned an unintentional background electron carrier concentration of 1×10^{16} cm^{-3} to prevent doping induced non-radiative recombination and impurity scattering. For electron blocking layer (EBL), a 10 nm p-doped $Al_{0.8}Ga_{0.2}N$ with hole concentration of 5×10^{17} cm^{-3} is used. A thin p-$Al_{0.4}Ga_{0.6}N$ layer is inserted between the EBL and the p-cladding to improve hole injection. The p-cladding consists of Mg-doped GaN with hole concentration of 7×10^{18} cm^{-3}.

The material parameters of AlGaN ternary alloys are expressed as

$$X(Al_xGa_{1-x}N) = x.\ X(AlN) + (1-x).X(GaN) - b.x.(1-x)$$

where, b is the bowing factor and X(AlN) and X(GaN) are the material parameters of binaries AlN and GaN with values mentioned in Table 1 [10].

Other simulation parameters, such as effective masses for carriers, elastic, piezoelectric, deformation potentials and 6×6 $k \cdot p$ parameters for ternary compound, were extrapolated linearly [16]. The valence band offset was set to 850 meV for GaN layer lattice matched to AlN, taking into account strain and polarization induced band bending effect. The operating temperature of the device is taken to be 300 K.

Doping dependent mobilities for the AlGaN were obtained using *Arora* modal, a built-in module for the numerical software [17]. The *Arora* model is introduced to depict the mobility as a function of carrier density, taking into account scattering by charged impurity ions

$$u(T, N_i) = u_{\min}^{n,p}\left(\frac{T}{T_o}\right)^{\alpha_m^{n,p}} + \frac{u_d^{n,p}\left(\frac{T}{T_o}\right)^{\alpha_d^{n,p}}}{1 + \left(\frac{N_D+N_A}{N_0^{n,p}\left(\frac{T}{T_o}\right)^{\alpha_N^{n,p}}}\right)^{A_a^{n,p}\left(\frac{T}{T_o}\right)^{\alpha_a^{n,p}}}}$$

where $u_{\min}$, u_d, α_m, α_d, α_N, α_a, N_0 are Arora model fitting parameters [18]. $N_A + N_D$ is the total concentration of ionized impurities. For electrons, fitting parameters are taken with dislocation density of 1×10^8 cm^{-2} [17]. Due to non-availability of data in current literature, the mobility fitting parameters for holes in AlN, are assumed to be same as of GaN in the *Arora* model.

3. Results and Discussion

To optimize the insertion layer, thickness and composition were varied. Different structures were simulated, as shown in Table 2. Structure A with no insertion layer (IL) is taken as reference.

To understand the recombination rates and carrier localization strength, carrier densities have to be studied in the active region. As shown in Fig. 2 are profiles of carrier concentration across the active region under forward bias conditions for different structures. An increase in hole density is observed with increase in Al mole fraction of the insertion layer. This enhancement in carrier density can be attributed to stronger confinement of hole in the active region. Shift of valence band to lower energies due to polarization induced fields is also seen with increase in insertion layer thickness

TABLE 2

Structures with insertion layers of different thicknesses and alloy composition

Structure	Al mole fraction in Insertion layer	Insertion Layer Thickness (nm)
A/Ref	0.55	-
B	0.7	0.25
C	0.8	0.25
D	0.9	0.25
E	1	0.25
F	0.8	0.5
G	0.9	0.5
H	1	0.5

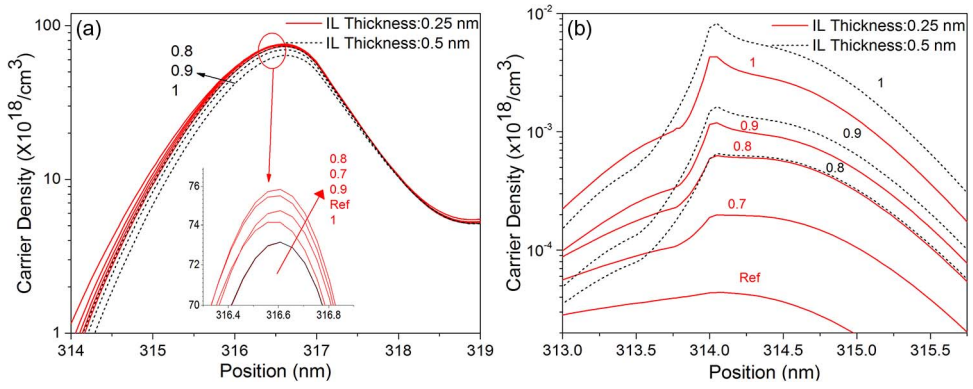

Fig. 2. Carrier densities of (a) electrons and (b) holes, under forward bias of 4.5 V, for insertion layer with different thicknesses and Al mole fraction.

leading to increase in hole density by a couple of magnitudes. In the reference structure, the small valence band offset can lead to overflow of holes into the n-side, adversely affecting the device performance. Thus the issue of hole leakage into n-cladding, for a single QW based device, is mitigated by using a insertion layer. A negligible change in the electron density profile is observed in the presence of insertion layer. The hole density increases with increase in the Al composition of the insertion layer as the valence band is shifted downwards.

When the carriers are injection into the active region, they can either recombine radiatively or non-radiatively. The recombination rates, in the simulation, are modeled as

$$R_{\text{Tot}} = R_{\text{Inj}} - (R_{\text{SRH}} + R_{\text{Auger}} + R_{\text{Direct}})$$

where

$$R_{\text{SRH}} = \frac{p.n - n_i^2}{\tau_p.(n + n_i) + \tau_n.(p + n_i)},$$
$$R_{\text{Auger}} = C_p.(n^2 - n_i^2).p + C_n.(p^2 - n_i^2).n,$$
$$R_{\text{Direct}} = C.(n.p - n_i^2)$$

where τ_n, τ_p, C_n and C_p are *Shockley–Read–Hall*, *Auger* and direct radiative recombination rates parameters, respectively. In the case of nitride based devices, *Auger* recombination term $C_p.n^2.p$ is dominant, due to a poor hole injection into the active region. The coefficients used in the simulation are shown in Table 3 [10], [19], [20]. At a lower carrier injection, the recombination is dominated by non-radiative recombination. With an increase in the forward bias, direct radiative recombination

TABLE 3

Parameters used to model *SRH*, *Auger* and direct radiative recombination rates

Binary Alloy	*Auger* Recombination Coefficients (cm^6s^{-1})		*SRH* Recombination Lifetimes (s)		Direct Radiative Recombination Coefficients (cm^3s^{-1})
	C_n	C_p	τ_n	τ_p	C
GaN	1.25×10^{-31}	5×10^{-32}	1×10^{-9}	20×10^{-9}	0.45×10^{-10}
AlN	5×10^{-32}	5×10^{-32}	5×10^{-9}	10×10^{-9}	0.18×10^{-10}

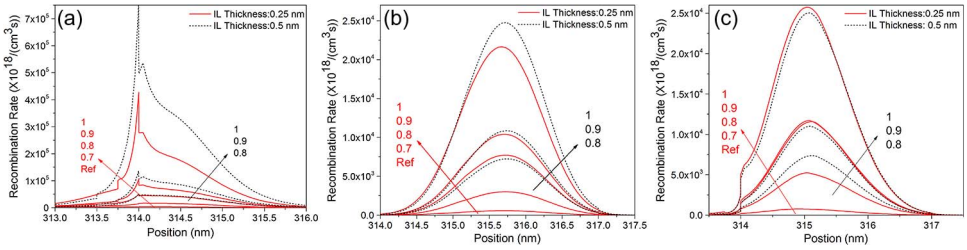

Fig. 3. Recombination rates of: (a) *SRH*, (b) *Auger* and (c) Direct, in the quantum well region (314 nm–317 nm) under forward bias of 4.5 V, for insertion layer with different thicknesses and Al concentrations. The solid red line and black dotted line represent the insertion layer (IL) thicknesses of 0.25 nm and 0.5 nm, respectively.

takes over. For high carrier injection, *Auger* recombination can be significant. *Auger* recombination rate has been considered as a dominant mechanism for efficiency rollover, or droop, in nitride based devices [21].

Since *Auger* recombination is a three particle process, an increase in carrier density increases the *Auger* recombination rate. For large bandgap material, the *Auger* recombination is suppressed due to smaller *Auger* recombination coefficients $< 10^{-31}$ cm^6s^{-1}. *SRH* recombination on the other hand is a single particle process and can be significant at lower carrier densities for large bandgap materials in which the trap states are closer to the center of the bandgap. For UV devices, both *SRH* and *Auger* can be significant and have to be taken into consideration in device design.

The recombination rates for the structures are shown in Fig. 3. A general trend of increase in recombination rates is observed with an increase in Al mole fraction in the insertion layer. This is due to the stronger carrier confinement and larger carrier density caused by polarization induced band bending. The *SRH* recombination is a single particle process and is caused by both holes and electrons being recombined through trap states. Since the hole concentration is more confined on bottom side of the well, cumulative *SRH* from both electron and holes peaks on that side. For nitride based devices, *Auger* recombination process is dominated by e-e-h transition due to higher electron density in the QW. Due to considerably larger electron density compared to that of holes, the *Auger* recombination follows the electron density profile. The abrupt changes in recombination profile across the active region are due to a change in recombination coefficients with composition. Direct recombination rates, being weighted by the spatial matrix element, maximizes for an AlN insertion layer of 0.25 nm thickness. Direct recombination decreases with further increases in thickness as the wavefunction overlap decreases with no significant improvement in carrier densities. Both *SRH* and *Auger* are seemed to be significant.

To understand the effectiveness of the AlGaN insertion layer, in enhancing hole confinement, the band diagram of reference structure A (no insertion layer) and structure C (with 0.25 nm thick $Al_{0.8}Ga_{0.8}N$ IL) are calculated and shown in Fig. 4(a) and (b), respectively. The valence band offset is increased by 203 meV in structure C as compared to the reference structure leading to stronger

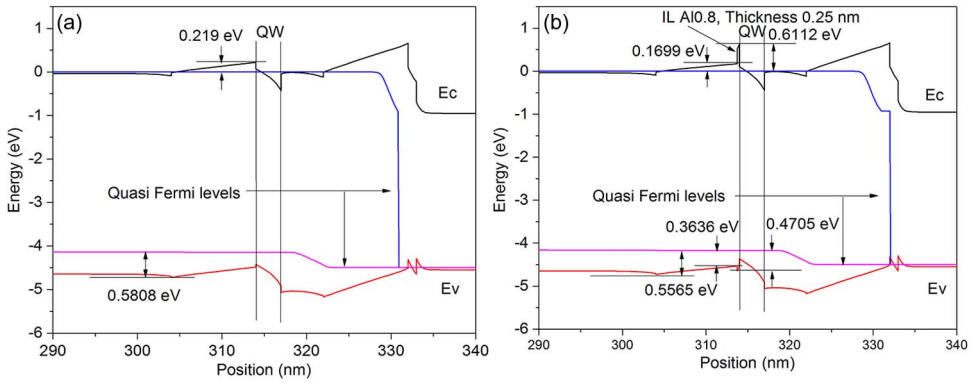

Fig. 4. Band diagram, under forward bias of 4.5V, for structure A and C.

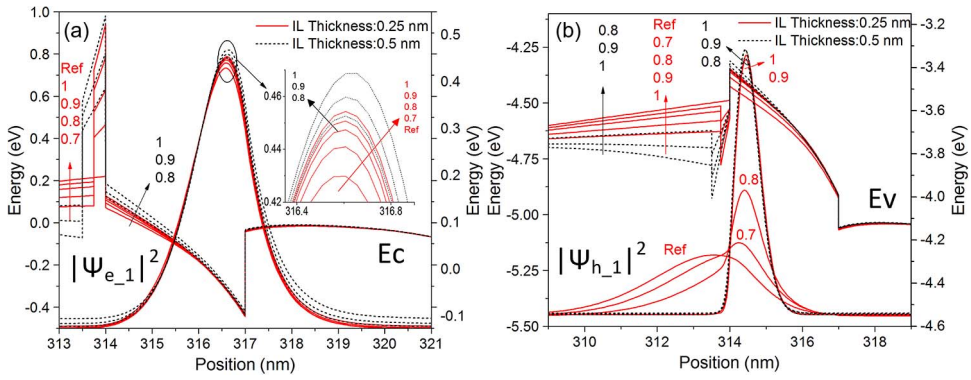

Fig. 5. Band diagram and wavefunction profiles corresponding to a) electron and b) holes, in the active region, for different structures. The fraction indicated, such as 0.7, 0.8, 0.9, and 1 are the Al compositions, and the Ref structure does not have the IL layer. The solid red line and black dotted line represent the insertion layer (IL) thicknesses of 0.25 nm and 0.5 nm, respectively.

hole confinement. In the reference structure, due to a lack of hole confinement, the hole leakage into the n-cladding can lead to non-radiative recombination. For conduction band, the energy barrier height introduced by the bottom barrier, is reduced from 219 meV to 169.9 meV leading to an improved electron injection in structure C. The bottom barrier is engineered to provide a positive electric field that forces holes back into the well, and leads to reduced hole leakage. The bandgap and thickness of top barrier are optimized to enhance electron confinement and avoid two dimensionless electron gas (2DEG) formation at the top barrier/EBL interface. In addition the asymmetric barrier-thicknesses are used to accommodate the differences in electron and hole mobilities.

The wavefunction profile gives an idea about the extent of carrier confinement in the active region and the strength of recombination. Fig. 5, shows the carrier wavefunctions with the corresponding band edges. For the reference structure, a valence band offset of 63 meV results in lack of hole confinement, causing the hole wave function to spread out into the barrier. In presence of an insertion layer, as shown in Fig. 4(b), confinement energy increases to 265 meV for structure C, causing the wave function to localize inside the well. For a 0.25 nm IL, increase in the insertion layer Al mole fraction, leads to increase in hole confinement as shown in Fig. 5(b). Therefore, insertion layer minimizes the hole overflow into the n-cladding. A decrease in wavefunction overlap was observed with thicker IL due to stronger bend bending and carriers confinement, at the bottom barrier well interface. A flip in electric field direction is observed, in the bottom barrier region, with increase in insertion layer thickness. In nitrides based heterointerfaces, difference in total

TABLE 4
Wavefunction overlap of carriers with different IL thicknesses and Al mole fraction

Structure	Wave function overlap $\lvert\langle\psi_{h\_1}\lvert\psi_{e\_1}\rangle\rvert^2$
A	0.0812
B	0.109
C	0.0925
D	0.0655
E	0.063
F	0.0547
G	0.0450
H	0.061

polarization fields, results in formation of fixed sheet charges. For a large bandgap material, under tensile strain on top of a small bandgap material, both spontaneous and piezoelectric polarization fields are in the negative c-direction, resulting in formation fixed positive sheet charge at the interface. The positive sheet charge can attract negative free carrier, thus resulting in a reduction or even flipping of electric field in the region at the interface. The maximum sheet carrier concentration at the interface, which is barrier-thickness dependent, increases with thickness [22]. This flip in electric field can adversely enhance hole leakage into n-doped layer. Taking conduction band into account, presence of the positive field creates a *2DEG* at the bottom barrier/IL interface for thicker ILs. The *2DEG* can act as a reservoir, from which the electrons can easily tunnel into the active region. The band bending also reduces the effective barrier height for electrons which enhances tunneling. The effect of IL on conduction band inside the QW, negligible shift in the electron wavefunction is seen. Beside the relatively insignificant effect on the electron distribution inside the quantum well, better confinement of the holes plays the major role in improving the device performance.

According to Fermi's golden rule, the transition matrix element is proportional to the square of the electron-hole wave function overlap or spatial overlap matrix element ($\lvert\langle\psi_{h\_1}\lvert\psi_{e\_1}\rangle\rvert^2$). With increase in overlap, the spontaneous radiative recombination is enhanced.

As shown in Fig. 5, the presence of the insertion layer shifts the hole wavefunction towards the quantum well. This reduction in charge separation in the quantum well, results in an enhancement of spatial matrix overlaps of more than 30% for structure B ($Al_{0.7}Ga_{0.3}N$ IL of thickness 0.25 nm) and more than 13% for structure C ($Al_{0.8}Ga_{0.2}N$ IL of thickness 0.25 nm) compared to ref structure (no IL). A thorough optimization of the insertion layer was performed to maximize spatial overlap parameter. With increase in overlap, the spontaneous radiative recombination is enhanced. Hence, this optimization is vital to improved device performance.

During the optimization of the insertion layer, well thickness was kept constant while composition was adjusted to keep the emission wavelength approximately 280 nm. For the reference structure the quantum states are non-localized causing a spread in wavefunction leading to smaller overlap. With an increase in the insertion layer height, the carrier confinement increases leading to the localized wavefunctions and the increase in wavefunctions overlap. Further increase in the Al mole fraction of the insertion layer leads to a confined quantum states with wavefunction localized at the insertion-QW interface. Stronger localization at the edge of the quantum well, due to large polarization fields, leads to a reduction in wavefunction overlap. For structure G ($Al_{0.9}Ga_{0.1}N$ with IL thickness of 0.5 nm), a slight spatial shift of electron wavefunction to the right results in reduction in overlap with that of holes (see Table 4).

A large band gap material layer adversely affects the electron injection into the QW by creating an energy barrier. The electrons can either tunnel or thermally excited over the barrier using $k_bT \sim 25$ meV energy from lattice. Since the effective mass of carrier is large in nitrides, there is a drastic decay of wavefunction inside the energy barrier layer thus greatly reducing tunneling

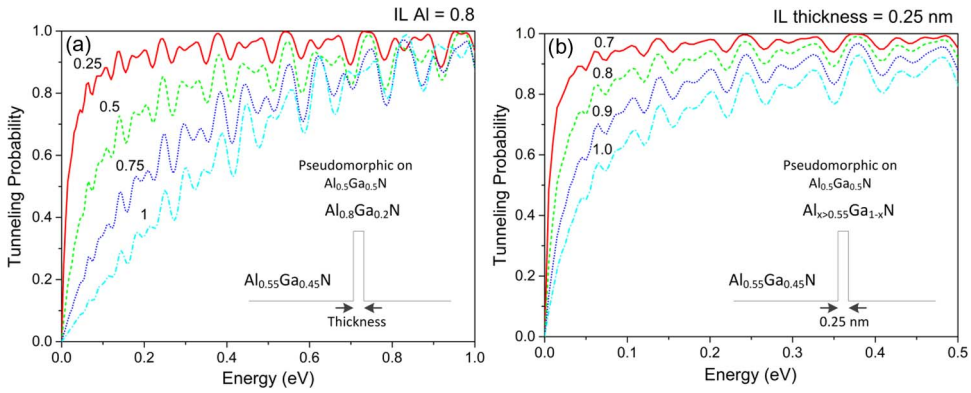

Fig. 6. (a) Tunneling probability, $T(E)$ for energy barriers with Al mole fraction of 0.8 with different IL thickness as indicated (b) the change in tunneling probability, $T(E)$, with increasing Al mole fraction in insertion layer with thickness of 0.25 nm$\sim$1 ML for structure B, C, D and E, with Al $= 0.7, 0.8, 0.9, 1$, respectively. Inset shows the rectangle barrier approximation for the $Al_{0.8}Ga_{0.2}N$ IL pseudomorphic on $Al_{0.5}Ga_{0.5}N$, for carrier tunneling probability $T(E)$ study, with varying insertion layer thicknesses.

current. This limits the barrier layer thickness to few monolayers. To study the effect of tunneling, the tunneling probability, $T(E)$, of a thin barrier layer was simulated under zero polarization fields (see Fig. 6). The band bending due to the polarization field is neglected for simplicity. To depict the real device the insertion layer is strained to $Al_{0.5}Ga_{0.5}N$. As seen from Fig. 5, under flatband condition, the insertion layer can be assumed to have a rectangular potential. For thicker insertion layers due to bend banding, the effective barrier height is considerably reduced thus the rectangular barrier approximation might not be very strong. However, this allows us to perform the tunneling studies for better IL design.

As shown in Fig 6(a), $T(E)$ decreases considerably with an increase in insertion layer thickness. In nitride material system, due to large carrier effective masses, decay of carrier wavefunction inside the barrier is quite strong. For 0.5 nm thick IL, and approximately 2 ML (mono-layer) thick $Al_{0.8}Ga_{0.2}N$ barrier, the tunneling probability is less than 10%, for carrier energies up to 25 meV. With a thinner insertion layer of 0.25 nm $\sim$1 ML, and with similar Al concentration, the tunneling probability increases to greater than 40%. This limits the insertion layer thickness to few monolayers, for effective electron injection into the QW. Fig. 6(b), shows the effect of Al mole fraction on $T(E)$ for a 0.25nm thick IL. The reduction in $T(E)$, with increase in Al mole fraction in the IL, is consistent with quantum mechanical analysis of energy barriers for large bandgap nitride materials. The ripple effect is observed due to resonant tunneling of electrons through quantum states supported in the quantum barrier system. In addition, the interference effects of incident and reflected wavefunctions at the barrier also led to this oscillation effect in the tunneling probability profile.

4. Conclusion

In this paper, we proposed a monolayer thick AlGaN insertion layer (IL), to enhance the device performance of a UV-LED design emitting at 280 nm. The numerical results show that the hole density can be increased based on stronger confinement and downward shift of the valence bands. The design without insertion layers suffers from high hole-leakage current and reduced spatial matrix overlap due to a spread in the hole-wavefunction into the barrier layer. The insertion layer increases the effective barrier height for the hole thus increasing their confinement and suppressing the hole spill-over and out of the active region. In addition, $T(E)$ modeling puts an upper limit of 2 ML for effective electron injection into the active region. An enhancement of more than 30% in the spatial matrix element was observed in structure C with insertion layer thickness of 0.25 nm $\sim$ 1 ML and Al concentration of 70%.

References

[1] J. Zhang, A. Chitnis, V. Adivarahan, S. Wu, V. Mandavilli, and R. Pachipulusu, "Milliwatt power deep ultraviolet light-emitting diodes over sapphire with emission at 278 nm," *Appl. Phys. Lett.*, vol. 81, no. 26, pp. 4910–4912, Dec. 2002.

[2] U. T. Schwarz, H. Braun, K. Kojima, Y. Kawakami, S. Nagahama, and T. Mukai, "Interplay of built-in potential and piezoelectric field on carrier recombination in green light emitting InGaN quantum wells," *Appl. Phys. Lett.*, vol. 91, no. 12, pp. 123503-1–123503-3, Sep. 2007.

[3] S.-H. Park and S.-L. Chuang, "Crystal-orientation effects on the piezoelectric field and electronic properties of strained wurtzite semiconductors," *Phys. Rev. B, Condens. Matter*, vol. 59, no. 7, pp. 4725–4737, 1999.

[4] S.-H. Park and S.-L. Chuang, "Comparison of zinc-blende and wurtzite GaN semiconductors with spontaneous polarization and piezoelectric field effects," *J. Appl. Phys.*, vol. 87, no. 1, pp. 353–364, Jan. 2000.

[5] S.-H. Park, "Crystal orientation effects on electronic properties of wurtzite GaN/AlGaN quantum wells with spontaneous and piezoelectric polarization," *Jpn. J. Appl. Phys.*, vol. 39, no. 6A, pp. 3478–3482, Jun. 2000.

[6] R. A. Arif, Y.-K. Ee, and N. Tansu, "Polarization engineering via staggered InGaN quantum wells for radiative efficiency enhancement of light emitting diodes," *Appl. Phys. Lett.*, vol. 91, no. 9, pp. 091110-1–091110-3, Aug. 2007.

[7] H. Zhao, G. Liu, J. Zhang, J. D. Poplawsky, V. Dierolf, and N. Tansu, "Approaches for high internal quantum efficiency green InGaN light-emitting diodes with large overlap quantum wells," *Opt. Exp.*, vol. 19, no. S4, pp. A991–A1007, Jul. 2011.

[8] S.-H. Park, D. Ahn, B.-H. Koo, and J.-W. Kim, "Dip-shaped InGaN/GaN quantum-well light-emitting diodes with high efficiency," *Appl. Phys. Lett.*, vol. 95, no. 6, pp. 063507-1–063507-3, Aug. 2009.

[9] M. Shatalov, W. Sun, A. Lunev, X. Hu, A. Dobrinsky, Y. Bilenko, J. Yang, M. Shur, R. Gaska, C. Moe, G. Garrett, and M. Wraback, "278 nm deep ultraviolet LEDs with 11% external quantum efficiency," in *Proc. 70th Annu. DRC*, 2012, pp. 255–256.

[10] J. Piprek, *Nitride Semiconductor Devices: Principles and Simulation*. Hoboken, NJ, USA: Wiley, 2007.

[11] S.-H. Park and S.-L. Chuang, "Spontaneous polarization effects in wurtzite GaN/AlGaN quantum wells and comparison with experiment," *Appl. Phys. Lett.*, vol. 76, no. 15, pp. 1981–1983, Apr. 2000.

[12] V. Fiorentini, F. Bernardini, and O. Ambacher, "Evidence for nonlinear macroscopic polarization in III–V nitride alloy heterostructures," *Appl. Phys. Lett.*, vol. 80, no. 7, pp. 1204–1206, Feb. 2002.

[13] G. Liu, J. Zhang, C.-K. Tan, and N. Tansu, "Efficiency-droop suppression by using large-bandgap AlGaInN thin barrier layers in InGaN quantum wells light-emitting diodes," *IEEE Photon. J.*, vol. 5, no. 2, p. 2201011, Apr. 2013.

[14] Y.-K. Kuo, T.-H. Wang, and J.-Y. Chang, "Advantages of blue InGaN light-emitting diodes with InGaN-AlGaN-InGaN barriers," *Appl. Phys. Lett.*, vol. 100, no. 3, pp. 031112-1–031112-3, Jan. 2012.

[15] S. Birner, S. Hackenbuchner, M. Sabathil, G. Zandler, J. Majewski, T. Andlauer, T. Zibold, R. Morschl, A. Trellakis, and P. Vogl, "Modeling of semiconductor nanostructures with nextnano^3," *Acta Phys. Polonica Ser. A*, vol. 110, no. 2, pp. 111–124, Aug. 2006.

[16] I. Vurgaftman and J. R. Meyer, "Electron band structure parameters," in *Nitride Semiconductor Devices: Principles and Simulation*. Hoboken, NJ, USA: Wiley, 2007, p. 13.

[17] N. D. Arora, J. R. Hauser, and D. J. Roulston, "Electron and hole mobilities in silicon as a function of concentration and temperature," *IEEE Trans. Electron Devices*, vol. ED-29, no. 2, pp. 292–295, Feb. 1982.

[18] E. Bellotti and F. Bertazzi, *Transport Parameters for Electrons and Holes*. Weinheim, Germany: Wiley-VCH Verlag GmbH & Co. KgaA, 2007.

[19] K. T. Delaney, P. Rinke, and C. G. Van de Walle, "Auger recombination rates in nitrides from first principles," *Appl. Phys. Lett.*, vol. 94, no. 19, pp. 191109-1–191109-3, May 2009.

[20] J. Piprek, *Semiconductor Optoelectronic Devices: Introduction to Physics and Simulation*. Amsterdam, The Netherlands: Elsevier, 2003.

[21] J. Iveland, L. Martinelli, J. Peretti, J. S. Speck, and C. Weisbuch, "Direct measurement of Auger electrons emitted from a semiconductor light-emitting diode under electrical injection: Identification of the dominant mechanism for efficiency droop," *Phys. Rev. Lett.*, vol. 110, no. 17, p. 177 406, Apr. 2013.

[22] O. Ambacher, J. Smart, J. R. Shealy, N. G. Weimann, K. Chu, M. Murphy, W. J. Schaff, L. F. Eastman, R. Dimitrov, L. Wittmer, M. Stutzmann, W. Rieger, and J. Hilsenbeck, "Two-dimensional electron gases induced by spontaneous and piezoelectric polarization charges in N- and Ga-face AlGaN/GaN heterostructures," *J. Appl. Phys.*, vol. 85, no. 6, pp. 3222–3233, Mar. 15, 1999.